*Desalination and Water Treatment*
www.deswater.com

doi:10.5004/dwt.2021.22346

226 (2021) 208–222
June

# Preparation of polyamine grafted silica gels supported naphthaldehyde Schiff's base and their adsorption properties as $Cu^{2+}$ ions adsorbents

Minghua Wang, Aili Wang*, Honglan Cai, Yuzhong Niu

*School of Chemistry and Materials Science, Ludong University, Yantai 264025, China, Tel. +86 178 6282 2690; email: wang.aili@mail.scut.edu.cn (A. Wang), Tel. +86 150 6638 7238; email: ytwmh@sohu.com (M. Wang)*

Received 26 September 2020; Accepted 4 March 2021

**ABSTRACT**

A series of silica gel supported naphthaldehyde modified amino-terminated polymers ($SiO_2$-APTS-NA, $SiO_2$-EDA-NA, $SiO_2$-DETA-NA, $SiO_2$-TETA-NA, and $SiO_2$-TEPA-NA) were synthesized and their structures were characterized by Fourier transform infrared, X-ray diffraction, elemental analysis, and porous structure analysis. The effect of different parameters including pH, contact time, coexisting metal ion, adsorbent dose, and initial concentrations of $Cu^{2+}$ ions on the adsorption were investigated. The isothermal adsorption behavior is fitted to the Langmuir model. The kinetics data indicated that the adsorption process of $Cu^{2+}$ ions on $SiO_2$-APTS-NA, $SiO_2$-EDA-NA, $SiO_2$-DETA-NA, $SiO_2$-TETA-NA, and $SiO_2$-TEPA-NA were governed by the film diffusion and followed the pseudo-second-order rate model. The adsorption capacity increased with the increase of the number of the amines in the functional groups. The adsorption behaviors of $Cu^{2+}$ ions on the five resins could be considered as spontaneous, endothermic, and chemical sorption process, resulting in their higher adsorption capacities at higher temperature.

*Keywords:* Synthesis; Functionalized silica gel; 2-Hydroxy-1-naphthaldehyde; Adsorption; $Cu^{2+}$

## 1. Introduction

Heavy metal ions removal from waters has attracted much attention due to the serious risk of these ions to human health and ecological systems [1]. Adsorption of toxic heavy metal ions on solid surfaces is considered to be an effective and economical method to improve the environment [2]. The adsorption uptake of heavy metal ions has been investigated by functionalizing the surface of various substrates, such as zeolite, activated carbon, resins, clays, and so on [3,4]. Some materials showed low absorption capacities.

Silica gel has been selected as the matrix due to its high surface area, nanometric pore size, excellent thermal, and mechanical stability, which has opened up a variety of applications across diverse fields [5,6]. In recent years, increasing attention has been paid to the chemical modification of the surface of silica gel with certain functional groups [7,8]. In our previous study, amino-terminated polyamines [9–11] and *m*-aramid and chitosan hybrid composite films [12] have been synthesized and confirmed.

Copper is one of the most widespread heavy metal contaminants in the environment. Up to now, some studies have been reported on the adsorption of $Cu^{2+}$ ions from an aqueous solution [13,14]. Chemical modification of silica surface by immobilization of Schiff bases covalently attached to silica gel has gained growing interest recently [15]. Therefore, in the present study, 2-hydroxy-1-naphthaldehyde as a simple chelating compound was loaded directly on the surface of silica gel by chemical immobilization in order to form two newly modified silica phases with O, N and O, O donor centers to improve the surface property and adsorption capacity of $Cu^{2+}$ ions.

The five silica gel derivatives were synthesized through the following steps: (1) introduce the amino

* Corresponding author.

groups onto the surface of silica gel; (2) Michael addition of methyl acrylate to γ-Aminopropyltriethoxysilane grafted silica; (3) amidation of the terminal ester groups with ethylenediamine (EDA), diethylenetriamine (DETA), triethylenetetramine (TETA), and tetraethylenepentamine (TEPA), respectively; (4) and then functionalized by the reaction with 2-Hydroxy-1-naphthaldehyde to obtain the products and their application for the adsorption of $Cu^{2+}$ ions from aqueous media were studied by the batch method.

## 2. Experimental

### 2.1. Materials and methods

Silica gel of chromatographic grade (100–200 mesh, Qingdao Makall Group Co., Ltd., Shandong, China) was received, and γ-aminopropyltriethoxysilane (APTS, Aikeda Chemical Reagent Co., Ltd., Chengdu, China) was of analytical grade. Polyamine compounds include EDA, DETA, TETA, and TEPA were purchased from Damao Chemical Reagent Company (Tianjin, China). 2-Hydroxy-1-naphthaldehyde was obtained from Adamas Reagent Limited Company (Shanghai, China). Stock solution of $Cu^{2+}$ was prepared by dissolving analytical grade $Cu(NO_3)_2{\cdot}3H_2O$ (Ruijinte Chemical Co., Ltd., Tianjin, China) in distilled water. Analytical reagent grade metal salts ($Pb(NO_3)_2$, $Cd(NO_3)_2{\cdot}4H_2O$ and $Ni(NO_3)_2{\cdot}6H_2O$) were supplied by Tianjin Bodi Company (Tianjin, China) and used without further purification. Toluene and methyl acrylate (MA) were redistilled just before use. All the other reagents used were of analytical-reagent grade.

An infrared spectrum of silica gel was reported on a Nicolet MAGNA-IR550 spectrophotometer under the test conditions of potassium bromide pellets and then scanned 32 times with the resolution of 4 $cm^{-1}$. The X-ray diffraction (XRD) patterns of the resins were recorded on an X-ray diffractometer (D/max-2500VPC, Rigaku Corporation, Japan). C, H, and N contents were characterized by combustion on the Elementar VarioEL III instrument of Germany. The nitrogen adsorption–desorption measurements of all adsorbents were performed by an ASAP Micromeritics 2020 of American at 77 K. The concentration of $Cu^{2+}$ ions were measured on a GBC-932A atomic absorption spectrophotometer (AAS) made in Australia.

### 2.2. Synthesis of Schiff-base-functionalized silica gel

The ideal synthetic schemes were illustrated in Fig. 1.

#### 2.2.1. Preparation of $SiO_2$-APTS

At first, silica gels were activated with nitric acid ($HNO_3$:$H_2O$ = 1:1) at refluxing temperature for 3 h, hydrochloric acid (HCl:$H_2O$ = 1:1) at room temperature for 6 h, finally washed with distilled water till there was no $Cl^{-1}$ and dried in a muffle at 160°C for 6 h.

100.0 g of activated silica gel was added to 300 mL of a toluene solution and 100 mL of APTS. The reactant solution was stirred at 70°C for 24 h. The product was filtered off and transferred to a Soxhlet extraction apparatus for reflux-extraction in toluene and methanol for 6 h, respectively. The product was dried in a vacuum at 50°C over 48 h, referred to as $SiO_2$-APTS.

#### 2.2.2. Preparation of $SiO_2$-MA

80 g of $SiO_2$-APTS was reacted with 65 mL of MA in 100 mL of methanol. The mixture was refluxed under a nitrogen atmosphere for 3 d at 50°C. The solid was filtered, washed with methanol and tetrahydrofuran, and dried under vacuum at 50°C over 48 h to derive the product named $SiO_2$-MA.

#### 2.2.3. Preparation of $SiO_2$-APTS-NA

$SiO_2$-APTS (10 g) and naphthaldehyde (1.73 g) were added to 75 mL of toluene. After being stirred at 25°C for 8 h under nitrogen, the sample was filtered, washed with toluene and ethanol, and dried under vacuum at 50°C over 48 h to get the resin named $SiO_2$-APTS-NA.

#### 2.2.4. Preparation of $SiO_2$-EDA and $SiO_2$-EDA-NA

Under a nitrogen atmosphere, 35 g $SiO_2$-MA, 50 mL methanol, and 320 mL ethanediamine were added in a 1,000 mL flask and stirred at 50°C for 5 d. The resin was filtered off, washed thoroughly with methanol and tetrahydrofuran. The product named $SiO_2$-EDA was dried at 50°C under vacuum for over 48 h.

The suspension of $SiO_2$-EDA (10.0 g) and naphthaldehyde (1.73 g) in toluene (75 mL) was stirred in reflux condition at 25°C for 8 h under a nitrogen atmosphere. The collected solid was filtered and transferred to a Soxhlet extraction apparatus for reflux-extraction in toluene and ethanol for 12 h, respectively. Finally, the product ($SiO_2$-EDA-NA) was dried for 48 h at 50°C under vacuum.

#### 2.2.5. Preparation of $SiO_2$-DETA and $SiO_2$-DETA-NA

The reaction was carried out under a nitrogen atmosphere and involved 30 g of $SiO_2$-MA, 465 mL of diethylenetriamine, and 150 mL of methanol as solvent. The mixture was stirred at 50°C for 5 d. The solid ($SiO_2$-DETA) was filtered, extracted with methanol and tetrahydrofuran for 12 h, respectively.

10 g $SiO_2$-DETA, 1.73 g naphthaldehyde, and 75 mL toluene were added in a flask and stirred for 8 h at 25°C under a nitrogen atmosphere. The purification procedure of the product was similar to that of $SiO_2$-EDA-NA, and $SiO_2$-DETA-NA was obtained.

#### 2.2.6. Preparation of $SiO_2$-TETA and $SiO_2$-TETA-NA

The reaction involved 35 g of $SiO_2$-MA, 784 mL of triethylene tetramine and 150 mL methanol. The reactant mixture was stirred for 5 d at 50°C under a nitrogen atmosphere. The product named $SiO_2$-TETA was filtered, extracted, and dried under vacuum at 50°C over 48 h.

Under a nitrogen atmosphere, a mixture of 1.73 g of naphthaldehyde and 10 g of $SiO_2$-TETA were added to a 500 mL flask with 75 mL of toluene as solvent. The mixture was stirred at 25°C for 8 h to react sufficiently. The purification

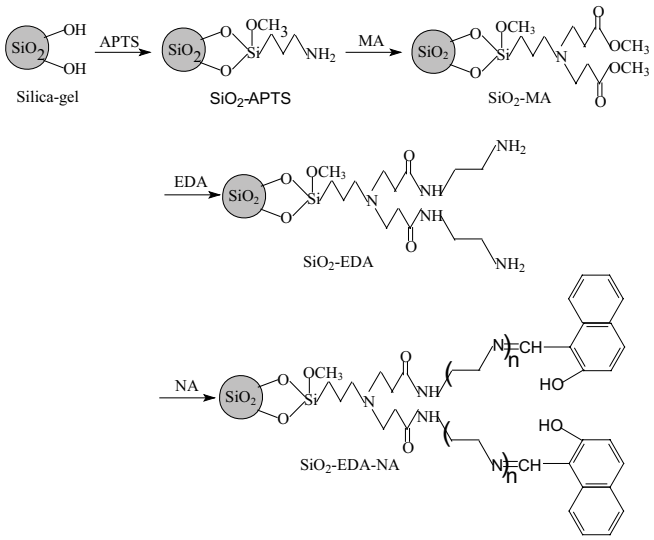


Fig. 1. Schematic expression of preparing process of the adsorbents ($n$ = 1–4).

procedure was similar to that of $SiO_2$-DETA-NA, and $SiO_2$-TETA-NA was obtained.

#### 2.2.7. Preparation of $SiO_2$-TEPA and $SiO_2$-TEPA-NA

Under a nitrogen atmosphere, 30 g of $SiO_2$-MA and 852 mL of tetraethylenepentamine reactant mixture was stirred for 5 d at 50°C in 150 mL of methanol solvent. The product $SiO_2$-TEPA was obtained.

A suspension of 10.0 g $SiO_2$-TEPA and 1.73 g naphthaldehyde in 75 mL of toluene was stirred and refluxed under nitrogen atmosphere for 8 h at 25°C. Then the product was filtered off and purified as that of the $SiO_2$-TETA-NA, after being dried under the vacuum at 50°C over 48 h, $SiO_2$-TEPA-NA was obtained.

### 2.3. Adsorption kinetics

Adsorption kinetics were performed by mixing 80.0 mg of the sorbents with 25 mL of $Cu^{2+}$ ions (0.002 mol $L^{-1}$) solution in a 100 mL Erlenmeyer flask at different temperatures. One milliliter of the solution was taken at different time intervals, where the residual concentration of $Cu^{2+}$ ions was determined via AAS.

### 2.4. Adsorption isotherm

Adsorption isotherms were studied by soaking 30 mg of the resins in a series of flasks containing 25 mL of different $Cu^{2+}$ ions concentrations. The mixture was shaken for 24 h at different temperatures and the concentration was determined via AAS.

## 3. Results and discussion

### 3.1. Fourier transform infrared characterization

The presence of the organic ligands covalently bonded to the silica gel was characterized by Fourier transform infrared (FTIR) absorption spectra. The main features on the surface of silica-gel were evidenced by the bands located at 1,100 $cm^{-1}$ (the intense band related to Si–O–Si stretching frequency of siloxane groups), 802 $cm^{-1}$ (the typical symmetric stretching of Si–O–Si of the mesoporous silica network) and 466 $cm^{-1}$ (the bending vibrations of Si–O–Si) [16]. The spectra of $SiO_2$-APTS showed the characteristic peak assigned to $–CH_2–$ stretching around 2,925 and 2,851 $cm^{-1}$, confirming the organic groups of APTS immobilized onto the surface of silica-gel. The presence of peaks in 1,743 $cm^{-1}$ (the symmetric stretching vibrations of C=O) confirms the attachment of MA onto $SiO_2$-APTS, indicating that esterification reaction occurred. After the reaction of $SiO_2$-MA with polyamines, the band at 1,743 $cm^{-1}$ for C=O disappeared, and a new band appeared at 1,561 $cm^{-1}$, which was characteristic of the primary amino group, due to the reaction of the ester groups in $SiO_2$-MA with EDA, DETA, TETA, and TEPA, respectively [17]. The characteristic peaks of aromatic (C=C) at 1,544 $cm^{-1}$ along with strong bands of azomethene stretching vibration (C=N) appeared at 1,635 $cm^{-1}$ in the FTIR spectra of $SiO_2$-APTS-SA, $SiO_2$-EDA-SA, $SiO_2$-DETA-SA, $SiO_2$-TETA-SA, and $SiO_2$-TEPA-SA, indicating Schiff's base formation [18].

### 3.2. Elemental analysis

The nitrogen, carbon, and hydrogen amount of the functionalized silica gel was determined by elemental analysis as illustrated in Table 1. An analysis of the result indicated the fact that the N content increased with the increase of the chain length of polyamine, implying that increasing the number of the amino groups could affect the values of nitrogen. The nitrogen concentration of Schiff's base products was lower than that of the amino-terminated ones, indicating that naphthaldehyde was successfully grafted onto the silica gel surface after Michael's addition and amidation reactions.

### 3.3. XRD analysis

Fig. 2 shows the XRD patterns of the absorbents. The low 2θ values for the materials were about 23°, which is assigned to the diffraction of the amorphous structures of the silica gel. It can be observed from Fig. 2, that there was no essential change in the topological structure of silica gel before and after the modification process. On the other hand, there is no novel diffraction peak appeared indicated that amino loaded samples and naphthaldehyde modified resins were completely amorphous.

### 3.4. Nitrogen adsorption–desorption isotherms

Fig. 3 shows the BJH desorption pore size distributions of silica gel and its derivatives. As shown in Fig. 3, the pores between 20 and 80 nm were dominant for all samples. With the proceeding of functionalization, the pore size distribution moved to the smaller pore size.

The porous structure parameters of the resins on the basis of the nitrogen adsorption data were summarized in Table 2. As presented in Table 2, the values of Brunauer–Emmett–Teller (BET) surface area, Barrett–Joyner–Halenda

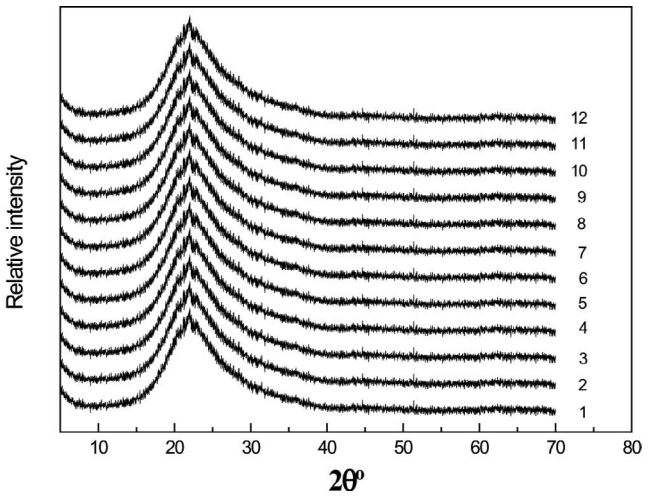


Fig. 2. XRD patterns of (1) $SiO_2$, (2) $SiO_2$-APTS, (3) $SiO_2$-MA, (4) $SiO_2$-EDA, (5) $SiO_2$-DETA, (6) $SiO_2$-TETA, (7) $SiO_2$-TEPA, (8) $SiO_2$-APTS-NA, (9) $SiO_2$-EDA-NA, (10) $SiO_2$-DETA-NA, (11) $SiO_2$-TETA-NA, and (12) $SiO_2$-TEPA-NA.

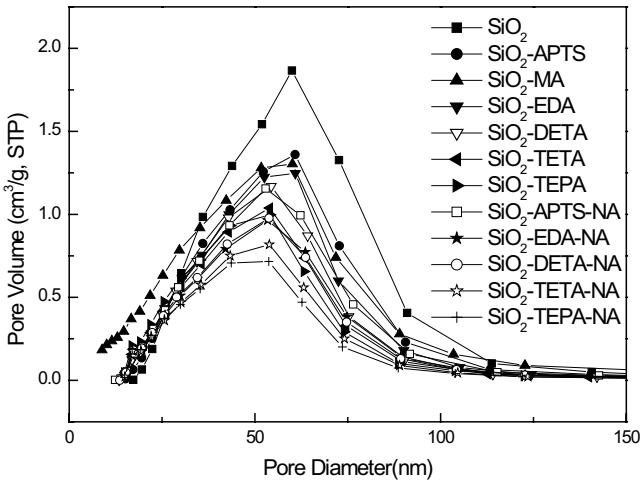


Fig. 3. BJH desorption pore size distributions of the products.

Table 1
Elemental analysis of the resins

| Resins | N (W%) | C (W%) | H (W%) |
|---|---|---|---|
| $SiO_2$-APTS | 0.93 | 3.06 | 1.41 |
| $SiO_2$-EDA | 2.14 | 5.93 | 1.18 |
| $SiO_2$-DETA | 2.58 | 8.07 | 0.61 |
| $SiO_2$-TETA | 3.25 | 8.12 | 1.71 |
| $SiO_2$-TEPA | 3.28 | 8.05 | 1.56 |
| $SiO_2$-APTS-NA | 0.80 | 7.46 | 0.93 |
| $SiO_2$-EDA-NA | 2.05 | 9.64 | 1.23 |
| $SiO_2$-DETA-NA | 2.54 | 9.77 | 1.31 |
| $SiO_2$-TETA-NA | 3.14 | 11.49 | 1.51 |
| $SiO_2$-TEPA-NA | 3.21 | 11.3 | 1.60 |

(BJH) desorption cumulative volume, and BJH desorption average pore radius of pores decreased gradually along with the functionalization reactions. This is probably because the volume of naphthaldehyde modified silica gel increased with the increase of molecular chain length of polyamines, the organic groups can easily fill the uniform micropores and thus restrict the access of nitrogen into the interior of silica gel.

Nitrogen adsorption–desorption isotherms for the resins are shown in Fig. 4. The silica gel and its derivatives were characterized by type IV nitrogen adsorption–desorption isotherms with H1 hysteresis loop [19,20], indicating their mesopore channels and narrow pore size distributions. The volume adsorbed for the resins sharply increased at a relative pressure ($P/P_0$) of approximately 0.6, representing capillary condensation taking place in the mesopores and the steepness reveals the uniformity of the mesopore sizes. The inflection position shifted toward lower relative pressures and the volume of nitrogen adsorbed mainly decreased with functionalization.

Table 2
Parameters of the porous structure of the resins

| Resins | BET surface area ($m^2/g$) | BJH desorption cumulative volume of pores ($cm^3/g$)* | BJH desorption average pore diameter (nm) |
|---|---|---|---|
| $SiO_2$ | 206.83 | 0.74 | 51.11 |
| $SiO_2$-APTS | 164.55 | 0.57 | 46.14 |
| $SiO_2$-MA | 163.80 | 0.54 | 45.95 |
| $SiO_2$-EDA | 159.81 | 0.51 | 41.71 |
| $SiO_2$-DETA | 146.19 | 0.49 | 42.63 |
| $SiO_2$-TETA | 140.74 | 0.45 | 41.11 |
| $SiO_2$-TEPA | 139.73 | 0.43 | 37.44 |
| $SiO_2$-APTS-NA | 167.45 | 0.50 | 42.74 |
| $SiO_2$-EDA-NA | 150.89 | 0.41 | 39.91 |
| $SiO_2$-DETA-NA | 140.04 | 0.41 | 39.32 |
| $SiO_2$-TETA-NA | 118.29 | 0.37 | 38.42 |
| $SiO_2$-TEPA-NA | 110.00 | 0.32 | 36.90 |

*Total volume of pores between 1.7 and 300 nm diameter.

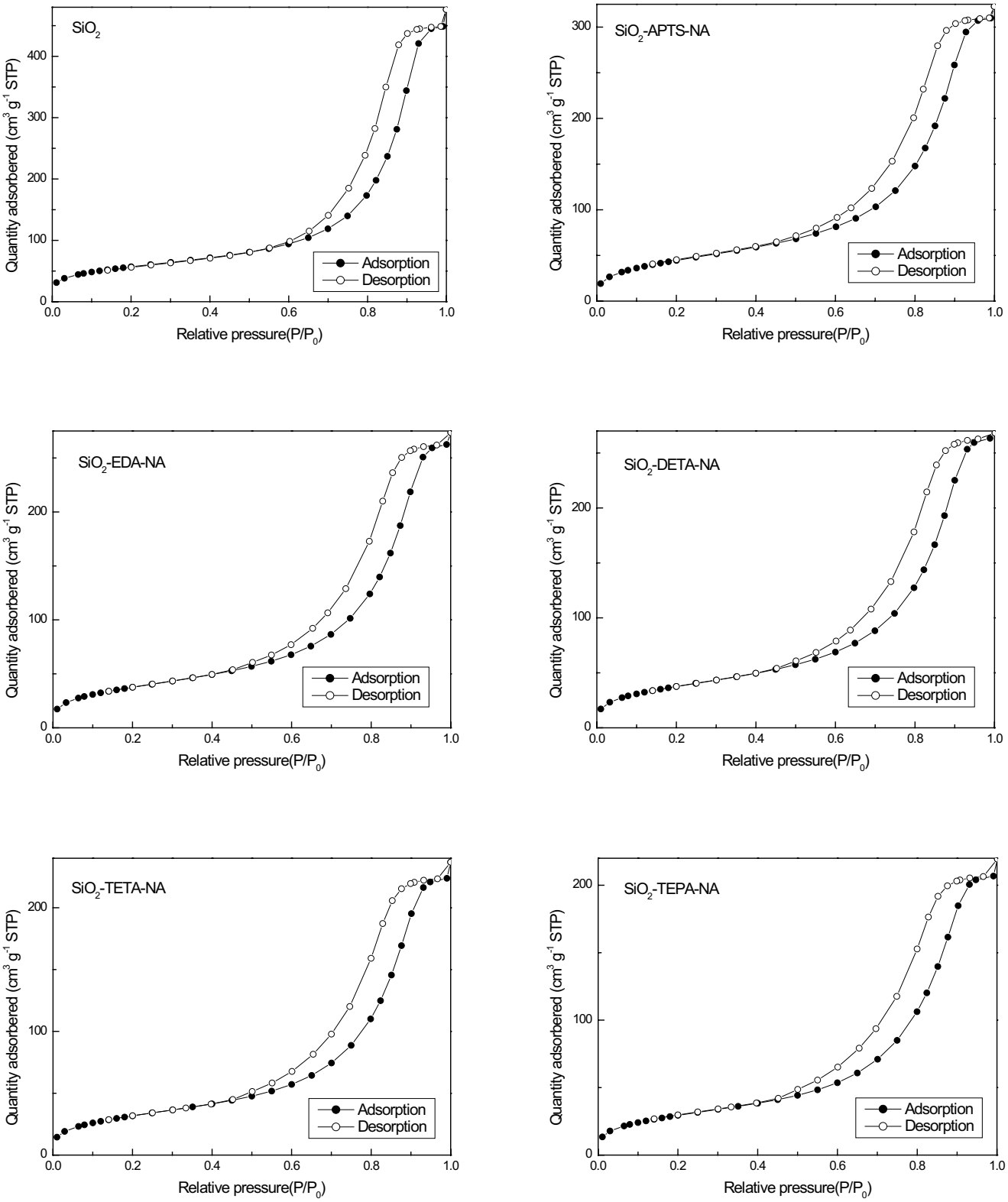


Fig. 4. Nitrogen adsorption–desorption isotherms of $SiO_2$, $SiO_2$-APTS-NA, $SiO_2$-EDA-NA, $SiO_2$-DETA-NA, $SiO_2$-TETA-NA, and $SiO_2$-TEPA-NA.

### 3.5. Static adsorption capacity

The order of adsorption capacities for $Cu^{2+}$ ions was $SiO_2$-TEPA-NA (0.21 mmol $g^{-1}$) > $SiO_2$-TETA-NA (0.17 mmol $g^{-1}$) > $SiO_2$-DETA-NA (0.16 mmol $g^{-1}$) > $SiO_2$-EDA-NA (0.14 mmol $g^{-1}$) > $SiO_2$-APTS-NA (0.11 mmol $g^{-1}$). The adsorption capacities of $Cu^{2+}$ ions adsorbed on the five kinds of resins increased with the increase of the length of the polyamine, indicating that the amino groups worked as adsorption sites for the metal cations effectively.

The comparison of adsorption capacities with those of the previously reported adsorbents is conducted by selecting $SiO_2$-TEPA-NA as the model and presented in Table 3. $SiO_2$-TEPA-NA is found to display competitive adsorption performance for $Cu^{2+}$ ions and the adsorption capacity is larger than most of the adsorbents reported previously. The results indicated that the five resins exhibited comparable adsorption efficiency and were promising adsorption materials for the effective removal of $Cu^{2+}$ ions from an aqueous solution.

### 3.6. Influence of pH

The solution pH value is one of the major factors influencing the adsorption of $Cu^{2+}$ ions. In this study, the effect of pH value on the extraction of $Cu^{2+}$ ions was performed and the results of extraction as a function of initial pH are presented in Fig. 5. The higher the pH value, the higher the adsorption amount. The adsorption capacities of the resins toward $Cu^{2+}$ ions increase with the increase in pH value. In acidic solution, most of N atoms of the amino groups in the chains of $SiO_2$-TEPA-NA, $SiO_2$-TETA-NA, $SiO_2$-DETA-NA, $SiO_2$-EDA-NA, and $SiO_2$-APTS-NA are protonated, the protonation degree of N atoms of amino groups decreases with the decline of acidity, so that the adsorption capacities of $Cu^{2+}$ ions increase with the rising of pH value.

### 3.7. Adsorption isotherms

The adsorption isotherms were studied for the relationship between equilibrium adsorption capacity and equilibrium concentration at a certain temperature. The isotherms for the sorption of $Cu^{2+}$ ions onto $SiO_2$-TEPA-NA, $SiO_2$-TETA-NA, $SiO_2$-DETA-NA, $SiO_2$-EDA-NA, and $SiO_2$-APTS-NA are shown in Fig. 6. It could be seen from Fig. 6 that the adsorption capacities of the five resins increased with the increase of temperature. At 5°C, 15°C, 25°C, and 35°C, it was clear that the adsorption capacities of $Cu^{2+}$ ions increased with the increase of the equilibrium concentration.

The Langmuir equation is applicable to homogeneous adsorption, where the adsorption of each adsorbate molecule onto the surface has equal adsorption activation energy. The Langmuir model was represented as [26]:

$$\frac{C_e}{q_e} = \frac{C_e}{q_0} + \frac{1}{q_0 b} \tag{1}$$

where $q_e$ is the adsorption capacity (mmol $g^{-1}$), $C_e$ is the equilibrium concentration of the $Cu^{2+}$ ions solution (mmol $L^{-1}$), $q_0$ is the saturated adsorption capacity (mmol $g^{-1}$), and $b$ is an empirical parameter (mL $mmol^{-1}$).

Table 3
Comparison of adsorption capacities of $Cu^{2+}$ ions on the products with other adsorbents reported in the literature

| Adsorbents | Adsorption capacities (mmol $g^{-1}$) | References |
|---|---|---|
| PPy/perlite | 0.056 | [21] |
| PE | 0.0041 | [22] |
| Natural zeolites | 0.035 | [23] |
| Virgin PA | 0.005 | [24] |
| Iron oxide on sand nanoparticles | 0.0198 | [25] |
| $SiO_2$-TEPA-NA | 0.21 | This work |

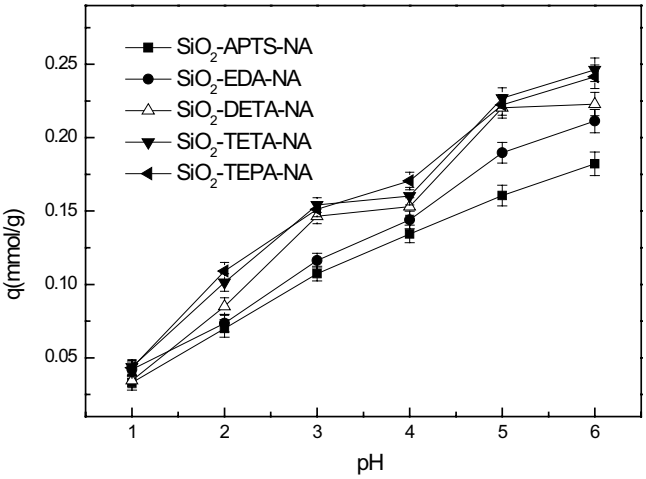


Fig. 5. Effect of pH on the adsorption of the resins for $Cu^{2+}$ ions.

The Freundlich equation is employed to describe heterogeneous systems and reversible adsorption and is not restricted to the formation of monolayers. The Freundlich isotherm model can be expressed as follows [27]:

$$\ln q_e = \ln K_F + \frac{1}{n} \ln C_e \tag{2}$$

where $q_e$ is the adsorption capacity (mmol $g^{-1}$), $C_e$ is the equilibrium concentration of the $Cu^{2+}$ ions solution (mmol $L^{-1}$), $n$ is the Freundlich constant, and $K_F$ is the binding energy constant reflecting the affinity of the resin to metal ions.

The parameters for the Langmuir and Freundlich isotherms obtained from Figs. S1 and S2 are presented in Table 4. It can be seen that the regression coefficient ($R_L^2$) obtained from the Langmuir model is higher than that ($R_F^2$) from the Freundlich model, suggesting that the Langmuir model can be employed to describe the adsorption isotherms of the five resins for $Cu^{2+}$ ions at the temperature range studied. In other words, the adsorption of $Cu^{2+}$ ions onto $SiO_2$-TEPA-NA, $SiO_2$-TETA-NA, $SiO_2$-DETA-NA, $SiO_2$-EDA-NA, and $SiO_2$-APTS-NA should be a monomolecular layer.

The constant $n$ in the Freundlich model represents the measure of both the relative magnitude and diversity of

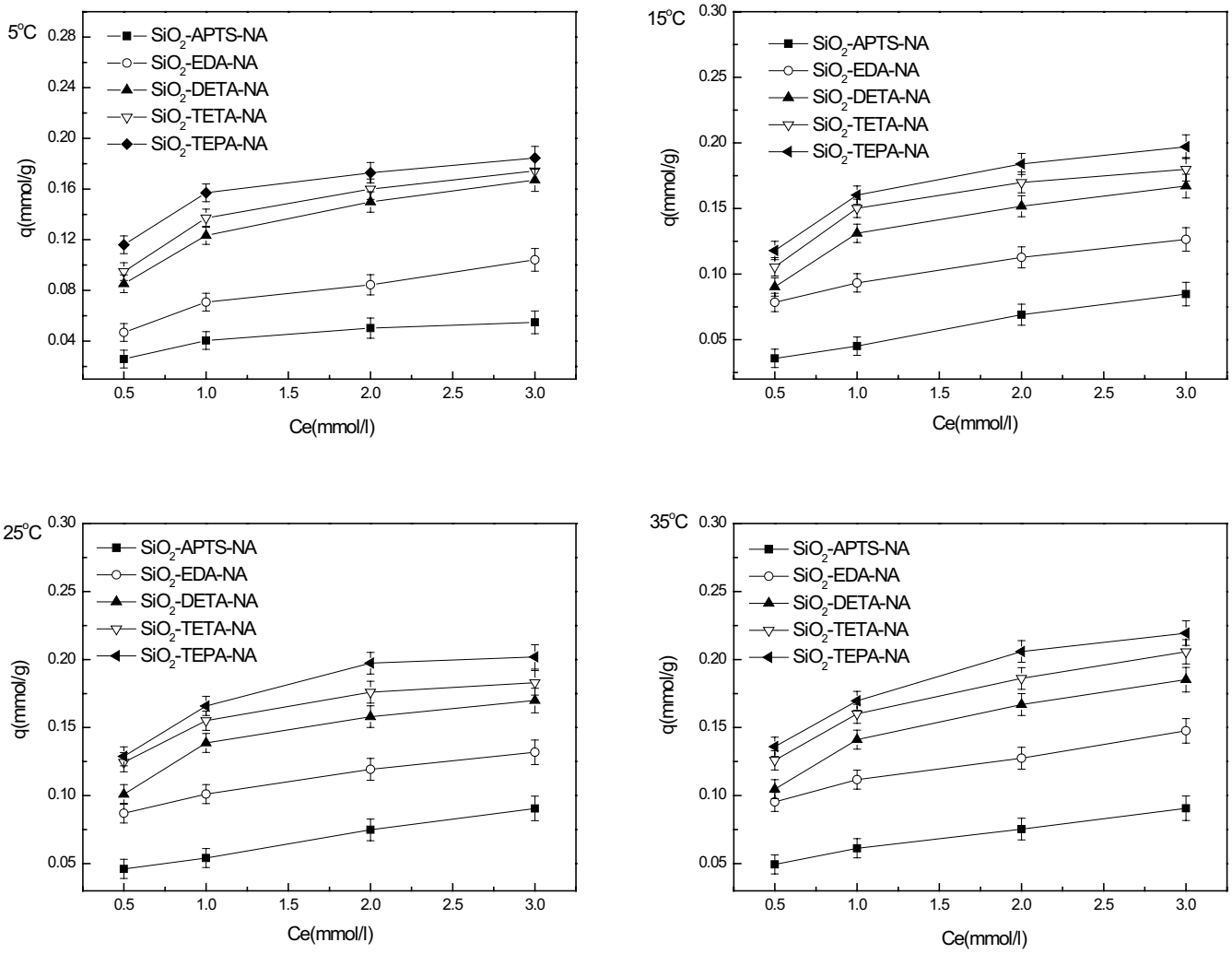


Fig. 6. Adsorption isotherms of the resins for $Cu^{2+}$ ions.

energies associated with $Cu^{2+}$ ions adsorption onto $SiO_2$-TEPA-NA, $SiO_2$-TETA-NA, $SiO_2$-DETA-NA, $SiO_2$-EDA-NA, and $SiO_2$-APTS-NA and the values of $1/n < 1$, suggesting the adsorption of the five resins for $Cu^{2+}$ ions were favorable [28].

### 3.8. Adsorption kinetics

Adsorption kinetics studies were carried out to determine the uptake rates of $Cu^{2+}$ ions on the resins and get access to the equilibrium time. Fig. 7 shows the adsorption kinetics of $SiO_2$-TEPA-NA, $SiO_2$-TETA-NA, $SiO_2$-DETA-NA, $SiO_2$-EDA-NA, and $SiO_2$-APTS-NA for $Cu^{2+}$ at 5°C–35°C.

As shown in Fig. 7, the adsorption capacities of the resins for $Cu^{2+}$ ions at 5°C–35°C increased with the extension of contact time. From these data, the equilibrium time for the adsorption of $Cu^{2+}$ under the given test conditions can be evaluated to be 3 h for the adsorbents. As can be seen from Fig. 7, the adsorption capacities increased with the increase of temperature. The order of adsorption capacities at a given temperature was: $SiO_2$-APTS-NA < $SiO_2$-EDA-NA < $SiO_2$-DETA-NA < $SiO_2$-TETA-NA < $SiO_2$-TEPA-NA, indicating the adsorption capacities increased with the increase of the N number of the polyamidoamine polymers.

The adsorption procedure of adsorbents for $Cu^{2+}$ ions is generally considered to take place through two mechanisms of film diffusion and particle diffusion. The experimental data were usually analyzed by Boyd [29] and Reichenberg [30] equations in order to distinguish film diffusion from particle diffusion-controlled adsorption. The relevant equations were given as follows:

$$F = 1 - \frac{6}{\pi^2}\sum_{n=1}^{\infty}\frac{1}{n^2}\exp\left(-\frac{D^i\pi^2 n^2 t}{r_0^2}\right) \tag{3}$$

or

$$F = 1 - \frac{6}{\pi^2}\sum_{n=1}^{\infty}\frac{1}{n^2}\frac{e^{-n^2 B_t}}{n^2} \tag{4}$$

where

$$B = \frac{\pi^2 D^i}{r_0^2} = \text{time constant} \tag{5}$$

Table 4
Parameters of Langmuir and Freundlich isotherm for adsorption of $Cu^{2+}$ ions on the adsorbents

| Adsorbents | $T$ | Langmuir | | | Freundlich | | |
|---|---|---|---|---|---|---|---|
| | | $q_0$ (mmol $g^{-1}$) | $b$ (mL $mmol^{-1}$) | $R_L^2$ | $K_F$ (mmol $g^{-1}$) | $1/n$ | $R_F^2$ |
| $SiO_2$-APTS-NA | | 0.0883 | 0.788 | 0.9987 | 1.5157 | 0.303 | 0.9737 |
| $SiO_2$-EDA-NA | | 0.1399 | 0.953 | 0.9918 | 1.5291 | 0.367 | 0.9862 |
| $SiO_2$-DETA-NA | 5°C | 0.2965 | 0.69 | 0.9996 | 1.4465 | 0.463 | 0.9847 |
| $SiO_2$-TETA-NA | | 0.3704 | 0.557 | 0.9994 | 1.3936 | 0.483 | 0.9725 |
| $SiO_2$-TEPA-NA | | 0.4698 | 0.362 | 0.9995 | 1.284 | 0.518 | 0.9596 |
| $SiO_2$-APTS-NA | | 0.0919 | 1.286 | 0.9923 | 1.6393 | 0.330 | 0.9922 |
| $SiO_2$-EDA-NA | | 0.2905 | 0.499 | 0.9987 | 1.3054 | 0.423 | 0.9967 |
| $SiO_2$-DETA-NA | 15°C | 0.3488 | 0.568 | 0.9992 | 1.3959 | 0.321 | 0.9723 |
| $SiO_2$-TETA-NA | | 0.4776 | 0.432 | 0.9993 | 1.3366 | 0.503 | 0.9577 |
| $SiO_2$-TEPA-NA | | 0.5146 | 0.439 | 0.9998 | 1.3247 | 0.527 | 0.9748 |
| $SiO_2$-APTS-NA | | 0.1210 | 0.957 | 0.9958 | 1.4663 | 0.351 | 0.988 |
| $SiO_2$-EDA-NA | | 0.3566 | 0.415 | 0.9983 | 1.2616 | 0.438 | 0.9996 |
| $SiO_2$-DETA-NA | 25°C | 0.4409 | 0.441 | 0.9997 | 1.3275 | 0.488 | 0.9715 |
| $SiO_2$-TETA-NA | | 0.5624 | 0.305 | 0.9999 | 1.2401 | 0.525 | 0.9789 |
| $SiO_2$-TEPA-NA | | 0.6126 | 0.374 | 0.9995 | 1.2929 | 0.544 | 0.9759 |
| $SiO_2$-APTS-NA | | 0.1517 | 0.718 | 0.9972 | 1.3924 | 0.359 | 0.9966 |
| $SiO_2$-EDA-NA | | 0.3689 | 0.448 | 0.9951 | 1.2649 | 0.456 | 0.9934 |
| $SiO_2$-DETA-NA | 35°C | 0.4945 | 0.551 | 0.9995 | 1.3668 | 0.498 | 0.9893 |
| $SiO_2$-TETA-NA | | 0.5994 | 0.461 | 0.9992 | 1.3087 | 0.536 | 0.9939 |
| $SiO_2$-TEPA-NA | | 0.6561 | 0.454 | 0.9998 | 1.3127 | 0.558 | 0.9941 |

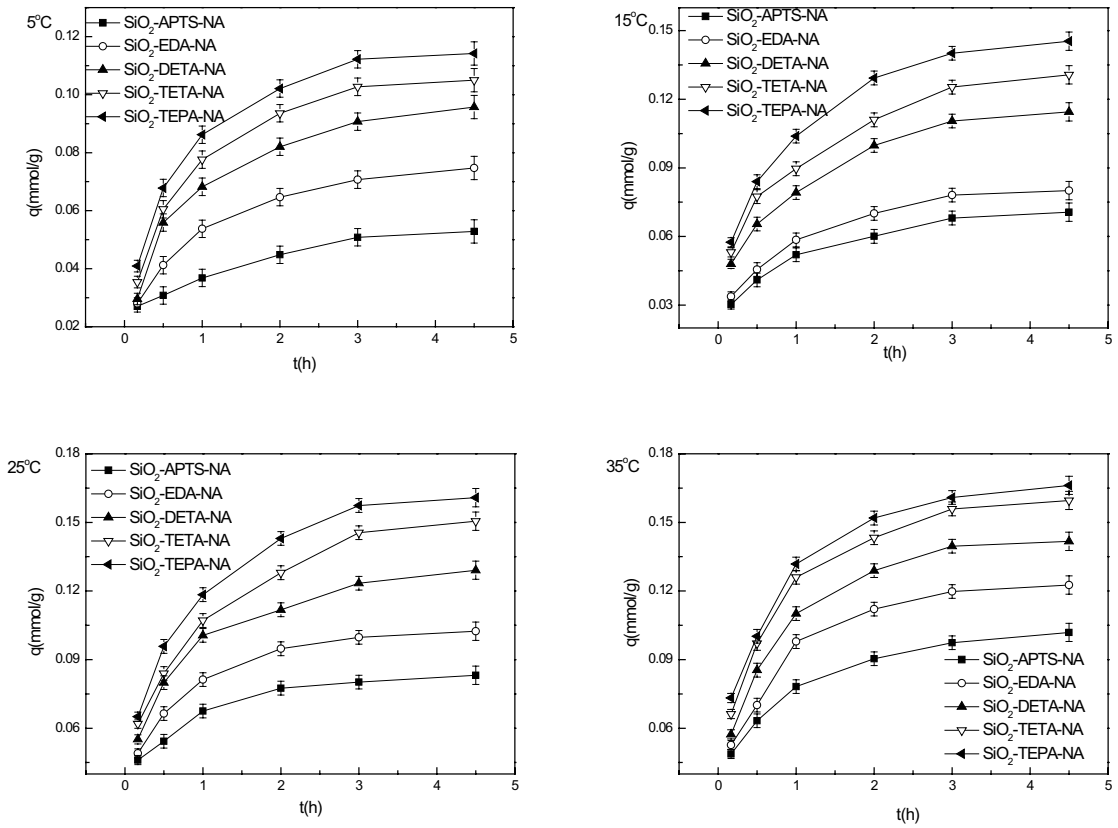


Fig. 7. Adsorption kinetics of $Cu^{2+}$ ions onto adsorbents at different temperature.

where $D^i$ is the effective diffusion coefficient of ion in the adsorbent phase; $r_0$ is the radius of the adsorbent particle, assumed to be spherical; and $n$ is an integer that defines the infinite series solution. $F$ is the fractional attainment of equilibrium at time $t$ and can be obtained by:

$$F = \frac{q_t}{q_0} \tag{6}$$

where $q_t$ is the amount of adsorbate taken up at time $t$ and is the maximum equilibrium uptake.

Values of $B_t$ can be obtained from corresponding values of $F$, and $B_t$ values for each $F$ given were plotted in Fig. S3 and the fitting results are shown in Table 5. Plots of $B_t$ vs. time of $Cu^{2+}$ ions onto $SiO_2$-TEPA-NA, $SiO_2$-TETA-NA, $SiO_2$-DETA-NA, $SiO_2$-EDA-NA, and $SiO_2$-APTS-NA at 5°C–35°C were used to distinguish between the film diffusion and particle diffusion-controlled adsorption. If the plots were straight line passing through the origin, the adsorption process should be dominated by the particle diffusion mechanism, otherwise, it might be governed by the film diffusion. As can be seen from Fig. S3, the lines of $B_t$ vs. time plots did not pass through the origin in the cases studied, indicating the film diffusion, not the particle diffusion, dominated the adsorption processes of $SiO_2$-TEPA-NA, $SiO_2$-TETA-NA, $SiO_2$-DETA-NA, $SiO_2$-EDA-NA, and $SiO_2$-APTS-NA for $Cu^{2+}$ ions.

To examine the controlling mechanism of adsorption processes such as chemical reaction and mass transfer, pseudo-first-order and pseudo-second-order kinetic models were used to test the experimental data as shown in Eqs. (7) and (8). The linear forms of pseudo-first-order and pseudo-second-order models were reported by Lagergren [31] and Ho [32]:

$$\log\left(q_e - q_t\right) = \log q_e - \frac{k_1}{2.303}t \tag{7}$$

$$\frac{t}{q_t} = \frac{1}{k_2 q_e^2} + \frac{1}{q_e}t \tag{8}$$

where $q_e$ (mmol $g^{-1}$) is the amount of metal adsorbed at equilibrium per unit weight of adsorbent, $q_t$ (mmol $g^{-1}$) is the adsorption capacity at time $t$, $k_1$ ($h^{-1}$) and $k_2$ (g $mmol^{-1}$ $h^{-1}$) are the rate constants of pseudo-first-order and pseudo-second-order adsorption.

The plots of $\log(q_e - q_t)$ vs. $t$ and $t/q_t$ vs. $t$ were employed to test the pseudo-first- and second-order models, and the results are shown in Fig. S4 and Fig. 8, respectively. The $k_1$, $k_2$, $q_e$ values, and the corresponding linear correlation coefficient $R_1^2$ and $R_2^2$ are given in Table 6.

The pseudo-second-order kinetic model is more adequate to depict the adsorption kinetics of $Cu^{2+}$ ions onto the five resins than the pseudo-first-order kinetic model as indicated by the linear plots (Fig. 8) with more superior correlation coefficients ($R_2^2$) and calculated adsorption capacity ($q_{e,cal}$). The result suggests that the upload of $Cu^{2+}$ ions by the adsorbents is dominated by the chemical interaction between the decorated silica gels and $Cu^{2+}$ ions.

Table 5
$B_t$ vs. time linear equations and coefficients $R^2$

| Resins | $T$ | Linear equation | $R^2$ |
|---|---|---|---|
| $SiO_2$-APTS-NA | | $B_t = 0.5952t + 0.1723$ | 0.9958 |
| $SiO_2$-EDA-NA | | $B_t = 0.7448t + 0.0284$ | 0.9996 |
| $SiO_2$-DETA-NA | 5°C | $B_t = 0.7165t + 0.0346$ | 0.9966 |
| $SiO_2$-TETA-NA | | $B_t = 0.8698t + 0.0138$ | 0.9999 |
| $SiO_2$-TEPA-NA | | $B_t = 0.8726t + 0.0181$ | 0.9993 |
| $SiO_2$-APTS-NA | | $B_t = 0.6534t + 0.1264$ | 0.9956 |
| $SiO_2$-EDA-NA | | $B_t = 0.7619t + 0.0595$ | 0.9996 |
| $SiO_2$-DETA-NA | 15°C | $B_t = 0.7405t + 0.0413$ | 0.9963 |
| $SiO_2$-TETA-NA | | $B_t = 0.6477t + 0.0896$ | 0.9969 |
| $SiO_2$-TEPA-NA | | $B_t = 0.8350t + 0.0063$ | 0.9980 |
| $SiO_2$-APTS-NA | | $B_t = 1.0093t + 0.1658$ | 0.9980 |
| $SiO_2$-EDA-NA | | $B_t = 0.9981t + 0.0966$ | 0.9999 |
| $SiO_2$-DETA-NA | 25°C | $B_t = 0.7055t + 0.1687$ | 0.9830 |
| $SiO_2$-TETA-NA | | $B_t = 0.6662t + 0.0787$ | 0.9995 |
| $SiO_2$-TEPA-NA | | $B_t = 0.8268t + 0.0440$ | 0.9998 |
| $SiO_2$-APTS-NA | | $B_t = 0.7745t + 0.1531$ | 0.9988 |
| $SiO_2$-EDA-NA | | $B_t = 0.9826t + 0.0249$ | 0.9943 |
| $SiO_2$-DETA-NA | 35°C | $B_t = 0.9454t + 0.0298$ | 0.9994 |
| $SiO_2$-TETA-NA | | $B_t = 0.8715t + 0.0865$ | 0.9943 |
| $SiO_2$-TEPA-NA | | $B_t = 0.9602t + 0.0567$ | 0.9977 |

Based on the data of pseudo-second-order kinetic model, it could be found that the orders of equilibrium adsorption capacities calculated ($q_{e,cal}$) at different temperatures are $SiO_2$-APTS-NA < $SiO_2$-EDA-NA < $SiO_2$-DETA-NA < $SiO_2$-TETA-NA < $SiO_2$-TEPA-NA, indicating that the adsorption capacities increased with the length of the polyamine chain at any temperatures, as mentioned before.

According to the theory of hard and soft acids and bases (HSAB) defined by Pearson, metal ions will have a preference for coordinating with ligands that have more or less same electronegative donor atoms. Based on the above analysis, the chelation model should be the dominating adsorption mechanism for $Cu^{2+}$ ions onto the resins. The possible chelation structure of $Cu^{2+}$ ions by the adsorbent is presented in Fig. 9.

### 3.9. Effect of adsorbent dose on the removal of $Cu^{2+}$ ions

Adsorbent dose is an important parameter influencing the adsorption processes since it determines the adsorption capacity of an adsorbent. To establish the effect of adsorbent dose on $Cu^{2+}$ ions adsorption from solution, the adsorption experiment was carried out via selecting $SiO_2$-DETA-NA as representative and using four adsorbent doses (10, 20, 30, and 40 mg) and the result is shown in Fig. 10.

It was apparent that the equilibrium adsorption amount increases with the increasing adsorbent dose, and then slows down. The removal percent of $Cu^{2+}$ ions increases with a raise of the adsorbent dose.

This result was anticipated because for a fixed initial solute concentration, the availability of surface area (or adsorption sites) increases with the increase of adsorbent

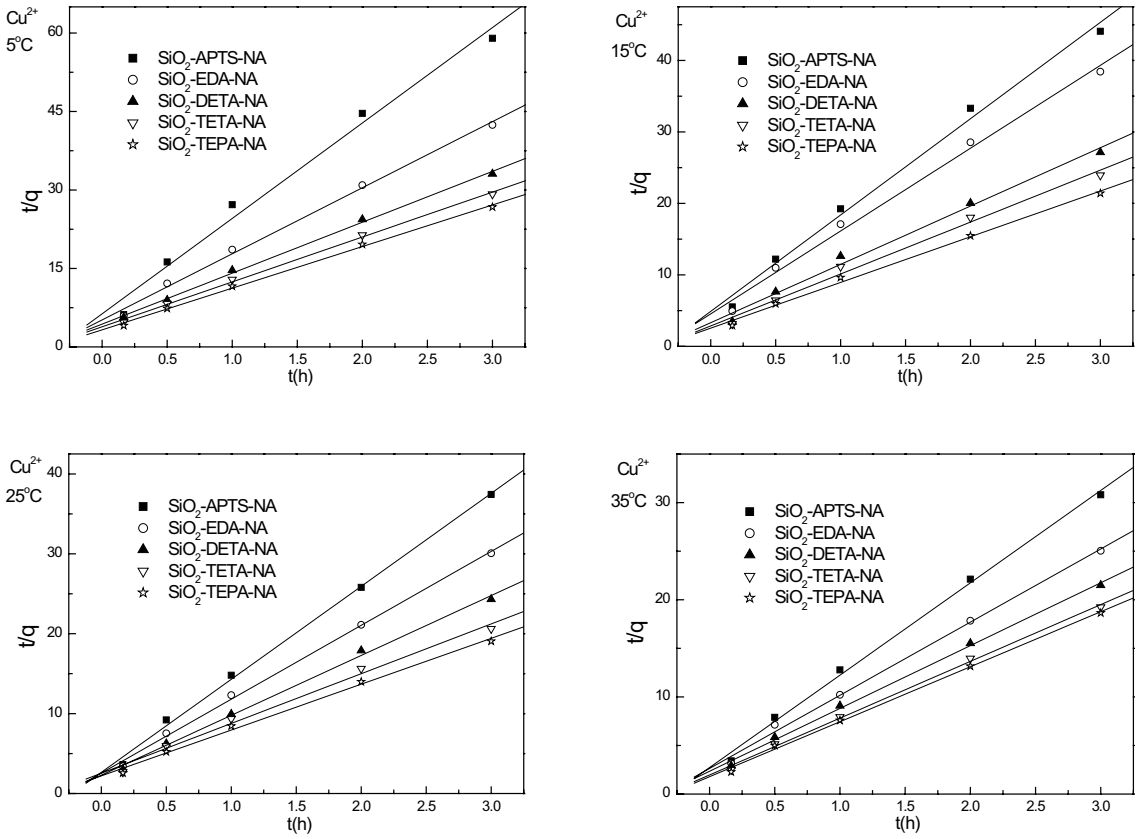


Fig. 8. Pseudo-second-order kinetic plots for the adsorption of $Cu^{2+}$ ions onto the resins at different temperatures.

Table 6
Adsorption kinetic parameters for the resins at different temperatures

| Adsorbents | $T$ | Pseudo-first-order kinetics | | | Pseudo-second-order kinetics | | |
|---|---|---|---|---|---|---|---|
| | | $k_1$ ($h^{-1}$) | $q_{e,cal}$ (mmol $g^{-1}$) | $R_1^2$ | $k_2$ (g $mmol^{-1}$ $h^{-1}$) | $q_{e,cal}$ (mmol $g^{-1}$) | $R_2^2$ |
| $SiO_2$-APTS-NA | | 0.88 | 0.0350 | 0.9805 | 52.68 | 0.0548 | 0.9930 |
| $SiO_2$-EDA-NA | | 0.85 | 0.0519 | 0.9978 | 30.94 | 0.0792 | 0.9980 |
| $SiO_2$-DETA-NA | 5°C | 0.86 | 0.0688 | 0.9950 | 21.74 | 0.1027 | 0.9989 |
| $SiO_2$-TETA-NA | | 1.15 | 0.0864 | 0.9920 | 19.17 | 0.1165 | 0.9990 |
| $SiO_2$-TEPA-NA | | 1.21 | 0.0936 | 0.9876 | 19.33 | 0.1257 | 0.9988 |
| $SiO_2$-APTS-NA | | 0.92 | 0.0491 | 0.9856 | 37.18 | 0.0742 | 0.9963 |
| $SiO_2$-EDA-NA | | 1.07 | 0.0612 | 0.9869 | 29.59 | 0.0863 | 0.9964 |
| $SiO_2$-DETA-NA | 15°C | 0.97 | 0.0847 | 0.9926 | 20.15 | 0.1225 | 0.9953 |
| $SiO_2$-TETA-NA | | 0.90 | 0.0934 | 0.9885 | 18.48 | 0.1376 | 0.9951 |
| $SiO_2$-TEPA-NA | | 0.98 | 0.1052 | 0.9986 | 16.03 | 0.1564 | 0.9974 |
| $SiO_2$-APTS-NA | | 0.92 | 0.0419 | 0.9939 | 51.18 | 0.0859 | 0.9988 |
| $SiO_2$-EDA-NA | | 1.05 | 0.0619 | 0.9989 | 33.60 | 0.1081 | 0.9990 |
| $SiO_2$-DETA-NA | 25°C | 0.85 | 0.0784 | 0.9904 | 24.53 | 0.1334 | 0.9985 |
| $SiO_2$-TETA-NA | | 0.97 | 0.1131 | 0.9847 | 15.27 | 0.1605 | 0.9953 |
| $SiO_2$-TEPA-NA | | 1.13 | 0.1245 | 0.9887 | 14.97 | 0.1742 | 0.9976 |
| $SiO_2$-APTS-NA | | 0.85 | 0.5948 | 0.9977 | 33.18 | 0.1052 | 0.9983 |
| $SiO_2$-EDA-NA | | 1.12 | 0.0860 | 0.9968 | 21.52 | 0.1328 | 0.9982 |
| $SiO_2$-DETA-NA | 35°C | 1.25 | 0.1113 | 0.9901 | 17.85 | 0.1546 | 0.9988 |
| $SiO_2$-TETA-NA | | 1.09 | 0.1110 | 0.9925 | 17.38 | 0.1711 | 0.9989 |
| $SiO_2$-TEPA-NA | | 1.00 | 0.1051 | 0.9985 | 17.97 | 0.1766 | 0.9989 |

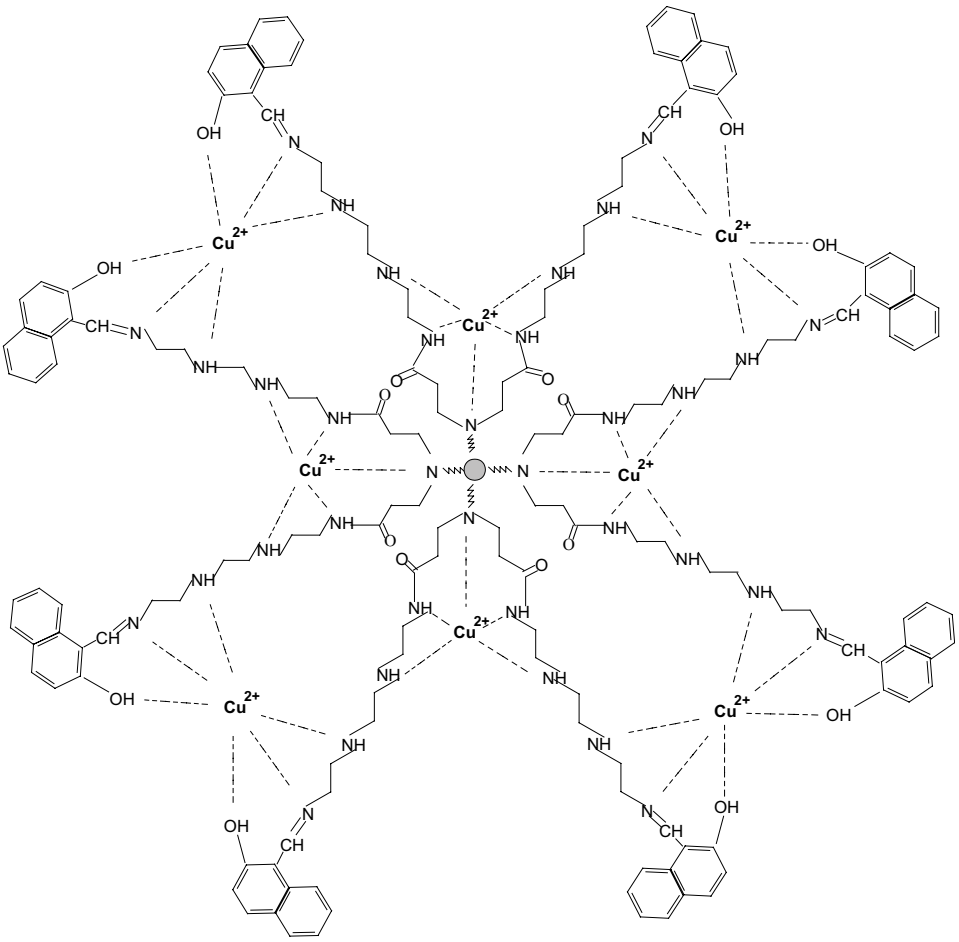


Fig. 9. Proposed structure of $Cu^{2+}$ ions chelation on the resin.

Table 7
Adsorption selectivity of the adsorbent for $Cu^{2+}$ ions

| System | Metal ions | Adsorption capacity (mmol $g^{-1}$) | Selective coefficient |
|---|---|---|---|
| $Cu^{2+}$-$Cd^{2+}$ | $Cu^{2+}$ | 0.08924 | 3.29 |
| | $Cd^{2+}$ | 0.02708 | |
| $Cu^{2+}$-$Pb^{2+}$ | $Cu^{2+}$ | 0.08692 | 2.64 |
| | $Pb^{2+}$ | 0.03298 | |
| $Cu^{2+}$-$Ni^{2+}$ | $Cu^{2+}$ | 0.08839 | 2.23 |
| | $Ni^{2+}$ | 0.03960 | |

dose, and then the binding sites are not fully utilized when the further increase in the sorbent dose, leading to the decrease of sorption ability [33,34].

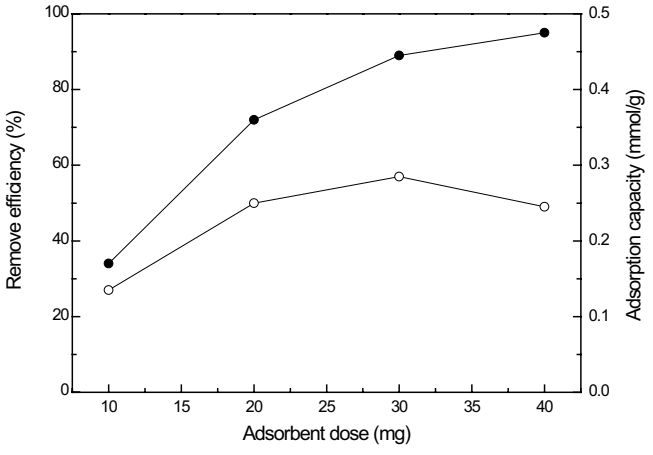


Fig. 10. Effect of adsorbent dose on the removal of $Cu^{2+}$ ions.

### 3.10. Adsorption selectivity

The adsorption selectivity of the adsorbent for $Cu^{2+}$ ions in aqueous solutions was investigated by selecting $SiO_2$-TETA-NA as the model, and the results are presented in Table 7. It can be seen from Table 7 that $SiO_2$-TETA-NA has excellent adsorption for $Cu^{2+}$ ions in the multinary solution of $Cu^{2+}$, $Cd^{2+}$, $Pb^{2+}$, and $Ni^{2+}$ ions. The selectivity of the adsorbent for $Cu^{2+}$ ions can be explained by the Irving–Williams series, which indicated higher metal complex stability of $Cu^{2+}$ ions than other divalent metal ions [35–37]. Thus, this novel composite material has good adsorption properties and high capacity for $Cu^{2+}$ ions and

can be applied for the pre-concentration and purification of $Cu^{2+}$ element in aqueous solutions containing metals.

### 3.11. Adsorption property for $Cu^{2+}$ ions from real aqueous solution

The application of the products for the removal of $Cu^{2+}$ ions from real samples such as sea water, tap water, and lake water was demonstrated by selecting $SiO_2$-DETA-NA as the model adsorbent. The adsorption capacity for $Cu^{2+}$ ions in sea water, lake water, tap water, and deionized water are 0.53, 0.59, 0.66, and 0.69 mmol·g$^{-1}$, respectively. The decrease of adsorption for $Cu^{2+}$ ions is mainly ascribed to the competition of $Na^+$, $K^+$, and $Ca^{2+}$ ions for the adsorption sites in real water systems, especially for that in the seawater [38].

## 4. Conclusions

A series of silica gel supported naphthaldehyde modified polyamidoamine polymers were prepared. Their structures were characterized by FTIR, XRD, elemental analysis, and porous structure analysis. The maximum adsorption capacities of $SiO_2$-APTS-NA, $SiO_2$-EDA-NA, $SiO_2$-DETA-NA, $SiO_2$-TETA-NA, and $SiO_2$-TEPA-NA for $Cu^{2+}$ ions were 0.11, 0.14, 0.16, 0.17, and 0.21 mmol g$^{-1}$ at 25°C, respectively.

The isotherm adsorption data of the $Cu^{2+}$ ions on adsorbents were well-fitted by the Langmuir model. The optimum pH corresponding to the maximum adsorption was found to be 6.0 for $SiO_2$-TEPA-NA, $SiO_2$-TETA-NA, $SiO_2$-DETA-NA, $SiO_2$-EDA-NA, and $SiO_2$-APTS-NA. The adsorption kinetic study indicated that the pseudo-second-order rate model provides an excellent fitting of the five resins for $Cu^{2+}$ ions.

## Acknowledgments

The authors are grateful for the financial support by the Natural Science Foundation of Shandong Province (ZR2019PB014) and the Industry, Education, and Research Cooperative Education Project of Ministry of Education of China (No. 201702068013).

## References

[1] J. Zhou, H. Zhou, Y. Zhang, J. Wu, H. Zhang, G. Wang, J. Li, Pseudocapacitive deionization of uranium(VI) with $WO_3$/C electrode, Chem. Eng. J., 398 (2020a) 125460–125468.
[2] P. Yin, Q. Xu, R. Qu, G. Zhao, Y. Sun, Adsorption of transition metal ions from aqueous solutions onto a novel silica gel matrix inorganic–organic composite material, J. Hazard. Mater., 173 (2010) 710–716.
[3] N. Ma, S. Chen, T. Li, Q. Zhang, Removal of mercury by an aminated fiber prepared by irradiation grafting copolymerization, Sep. Sci. Technol., 47 (2012) 867–874.
[4] U. Neubauer, B. Nowack, G. Furrer, R. Schulin, Heavy metal sorption on clay minerals affected by the siderophore desferrioxamine B, Environ. Sci. Technol., 34 (2000) 2749–2755.
[5] X. Song, Y. Niu, P. Zhang, C. Zhang, Z. Zhang, Y. Zhu, R. Qu, Removal of Co(II) from fuel ethanol by silica-gel supported PAMAM dendrimers: combined experimental and theoretical study, Fuel, 199 (2017) 9–101.
[6] S. Zhang, H. Gao, X. Xu, R. Cao, H. Yang, X. Xu, J. Li, MOF-derived CoN/N-C@$SiO_2$ yolk-shell nanoreactor with dual active sites for highly efficient catalytic advanced oxidation processes, Chem. Eng. J., 381 (2020) 122670–122681.
[7] S. Zhang, Y. Niu, Z. Chen, H. Chen, Z. Yang, L. Bai, B. Yuan, Removal of Fe(III) from ethanol by silica-gel supported ester-terminated PAMAM dendrimers: experimental and DFT calculation, Desal. Water Treat., 164 (2019) 310–318.
[8] M. Esmaeilpour, A.R. Sardarian, J. Javidi, Synthesis and characterization of Schiff base complex of Pd(II) supported on superparamagnetic $Fe_3O_4$@$SiO_2$ nanoparticles and its application as an efficient copper- and phosphine ligand-free recyclable catalyst for Sonogashira-Hagihara coupling reactions, J. Organomet. Chem., 749 (2014) 233–240.
[9] R. Qu, M. Wang, C. Sun, Y. Zhang, C. Ji, H. Chen, Y. Meng, P. Yin, Chemical modification of silica-gel with hydroxyl- or amino-terminated polyamine for adsorption of Au(III), Appl. Surf. Sci., 255 (2008) 3361–3370.
[10] R. Qu, M. Wang, R. Song, Ch. Sun, Y. Zhang, X. Sun, C. Ji, C. Wang, P. Yin, Adsorption kinetics and isotherms of Ag(I) and Hg(II) onto silica gel with functional groups of hydroxyl- or amino-terminated polyamines, J. Chem. Eng. Data, 56 (2011) 1982–1990.
[11] M. Wang, R. Qu, C. Sun, P. Yin, H. Chen, Dynamic adsorption behavior and mechanism of transition metal ions on silica gels functionalized with hydroxyl- or amino-terminated polyamines, Chem. Eng. J., 221 (2013) 264–274.
[12] M. Wang, R. Qu, C. Sun, Y. Niu, Y. Zhang, J. Gao, H. Cai, X. Song, Synthesis, characterization, and adsorption properties of *m*-aramid and chitosan hybrid composite flms with the ratio of 100/0, 85/15, 65/35, 50/50, and 35/65 toward Hg(II) ions, Desal. Water Treat., 146 (2019) 197–209.
[13] H. Yang, J. Fan, H. Tian, X. Wang, W. Fu, E. Alam, Synthesis of imprinted amino-functionalized mesoporous silica and their selective adsorption performance of $Pb^{2+}$, $Cu^{2+}$, and $Zn^{2+}$, J. Sol-Gel Sci. Technol., 90 (2019) 465–477.
[14] Y. Zhang, X. Cao, J. Sun, G. Wu, J. Wang, D. Zhang, Synthesis of pyridyl Schiff base functionalized SBA-15 mesoporous silica for the removal of Cu(II) and Pb(II) from aqueous solution, J. Sol-Gel Sci. Technol., 94 (2020) 658–670.
[15] M.A. Betiha, Y.M. Moustafa, M.F. El-Shahat, E. Rafik, Polyvinylpyrrolidone-Aminopropyl-SBA-15 schiff Base hybrid for efficient removal of divalent heavy metal cations from wastewater, J. Hazard. Mater., 397 (2020) 122675–122687.
[16] X.G. Wang, K.S.K. Lin, J.C.C. Chan, S. Cheng, Direct Synthesis and catalytic applications of ordered large pore aminopropyl-functionalized SBA-15 mesoporous materials, J. Phys. Chem. B, 109 (2005) 1763–1769.
[17] Y. Jiang, Q. Gao, H. Yu, Y. Chen, F. Deng, Intensively competitive adsorption for heavy metal ions by PAMAM-SBA-15 and EDTA-PAMAM-SBA-15 inorganic–organic hybrid materials, Microporous Mesoporous Mater., 103 (2007) 316–324.
[18] E.M. Soliman, M.E. Mahmoud, S.A. Ahmed, Synthesis, characterization and structure effects on selectivity properties of silica gel covalently bonded diethylenetriamine mono- and bis-salicyaldehyde and naphthaldehyde Schiff's bases towards some heavy metal ions, Talanta, 54 (2001) 243–253.
[19] K.S.W. Sing, D.H. Everett, R.A.W. Haul, L. Moscou, R.A. Pierotti, J. Rouquerol, T. Siemieniewska, Reporting physisorption data for gas/solid systems-with special reference to the determination of surface area and porosity, Pure Appl. Chem., 57 (1985) 603–619.
[20] M. Mureseanu, A. Reiss, N. Cioatera, I. Trandafir, V. Hulea, Mesoporous silica functionalized with 1-furoyl thiourea urea for Hg(II) adsorption from aqueous media, J. Hazard. Mater., 182 (2010) 197–203.
[21] A. Naghizadeh, S.J. Mousavi, E. Derakhshani, M. Kamranifar, S.M. Sharifi, Fabrication of polypyrrole composite on perlite zeolite surface and its application for removal of copper from wood and paper factories wastewater, Korean J. Chem. Eng., 35 (2018) 662–670.
[22] V. Godoy, G. Blázquez, M. Calero, L. Quesada, M.A. Martín-Lara, The potential of microplastics as carriers of metals, Environ. Pollut., 255 (2019) 113363–113374.
[23] N. Elboughdiri, The use of natural zeolite to remove heavy metals Cu(II), Pb(II) and Cd(II), from industrial wastewater, Cogent Eng., 7 (2020) 1782623–1782636.

[24] J. Yang, L. Cang, Q. Sun, G. Dong, S.T. Ata-Ul-Karim, D. Zhou, Effects of soil environmental factors and UV aging on $Cu^{2+}$ adsorption on microplastics, Environ. Sci. Pollut. Res., 26 (2019) 23027–23036.
[25] S. Lee, C. Laldawngliana, D. Tiwari, Iron oxide nano-particles-immobilized-sand material in the treatment of Cu(II), Cd(II) and Pb(II) contaminated waste waters, Chem. Eng. J., 195 (2012) 103–111.
[26] I. Langmuir, The adsorption of gases on plane surfaces of glass, mica and platinum, J. Am. Chem. Soc., 40 (1918) 1361–1403.
[27] H.M.F. Freundlich, Über die adsorption in lösungen, Z. Phys., 57 (1906) 385–470.
[28] A. Shahbazi, H. Younesi, A. Badiei, Functionalized SBA-15 mesoporous silica by melamine-based dendrimer amines for adsorptive characteristics of Pb(II), Cu(II) and Cd(II) heavy metal ions in batch and fixed bed column, Chem. Eng. J., 168 (2011) 505–518.
[29] G.E. Boyd, A.W. Adamson, L.S. Myers, The exchange adsorption of ions from aqueous solutions by organic zeolites. II. Kinetics, J. Am. Chem. Soc., 69 (1947) 2836–2848.
[30] D. Reichenberg, Properties of ion-exchange resins in relation to their structure. III. Kinetics of exchange, J. Am. Chem. Soc., 75 (1953) 589–597.
[31] S. Lagergren, Zur theorie der sogenannten adsorption geloster stoffe, Kungl. Svens. Vetenskapsakad. Handl., 24 (1898) 1–39.
[32] Y.S. Ho, G. McKay, Pseudo-second order model for sorption processes, Process Biochem., 34 (1999) 451–465.
[33] A.A. Hussain, S. Nazir, R. Irshad, K. Tahir, M. Raza, Z.U.H. Khan, A.U. Khan, Synthesis of functionalized mesoporous Ni-SBA-16 decorated with MgO nanoparticles for Cr(VI) adsorption and an effective catalyst for hydrodechlorination of chlorobenzene, Mater. Res. Bull., 133 (2021) 111059–111067.
[34] H. He, X. Meng, Q. Yue, W. Yin, Y. Gao, P. Fang, L. Shen, Thiol-ene click chemistry synthesis of a novel magnetic mesoporous silica/chitosan composite for selective Hg(II) capture and high catalytic activity of spent Hg(II) adsorbent, Chem. Eng. J., 405 (2021) 126743–126756.
[35] J. Kang, S. Lee, H. Jang, S. Kim, Synthesis of poly(ethyleneimine)-functionalized mesoporous silica gel with dual loading of host ion and crosslinking for enhanced heavy metal removal in multinary solutions, Microporous Mesoporous Mater., 311 (2021) 110698–110706.
[36] W.D. Henry, D. Zhao, A.K. SenGupta, C. Lange, Preparation and characterization of a new class of polymeric ligand exchangers for selective removal of trace contaminants from water, React. Funct. Polym., 60 (2004) 109–120.
[37] M.S. Kandanapitiye, F.J. Wang, B. Valley, C. Gunathilake, M. Jaroniec, S.D. Huang, Selective ion exchange governed by the Irving–Williams series in $K_2Zn_3[Fe(CN)_6]_2$ nanoparticles: toward a designer prodrug for wilson's disease, Inorg. Chem., 54 (2015) 1212–1214.
[38] Y. Zhou, L. Luan, B. Tang, Y. Niu, R. Qu, Y. Liu, W. Xu, Fabrication of Schiff base decorated PAMAM dendrimer/magnetic $Fe_3O_4$ for selective removal of aqueous Hg(II), Chem. Eng. J., 398 (2020b) 125651–125662.

## Supporting information

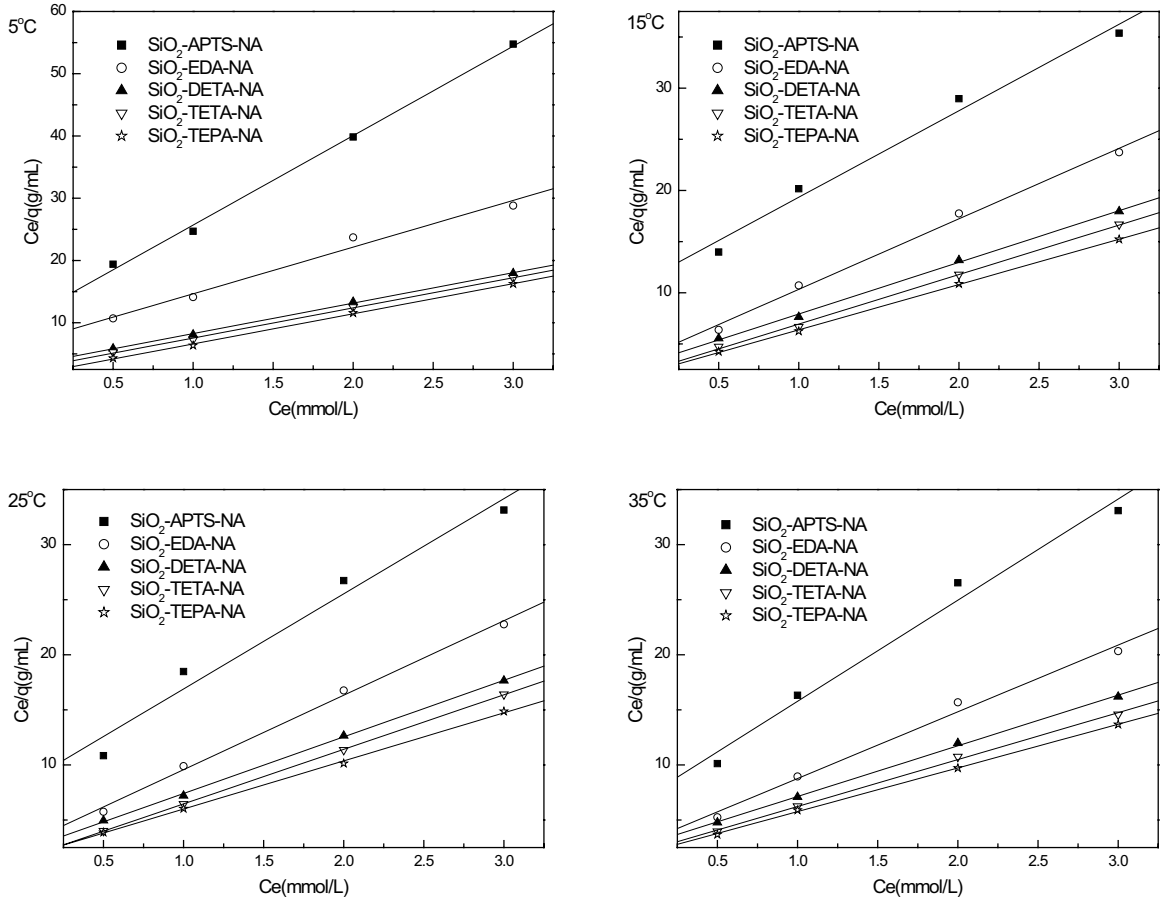


Fig. S1. Langmuir isotherms of $Cu^{2+}$ ions adsorbed on the resins at different temperature.

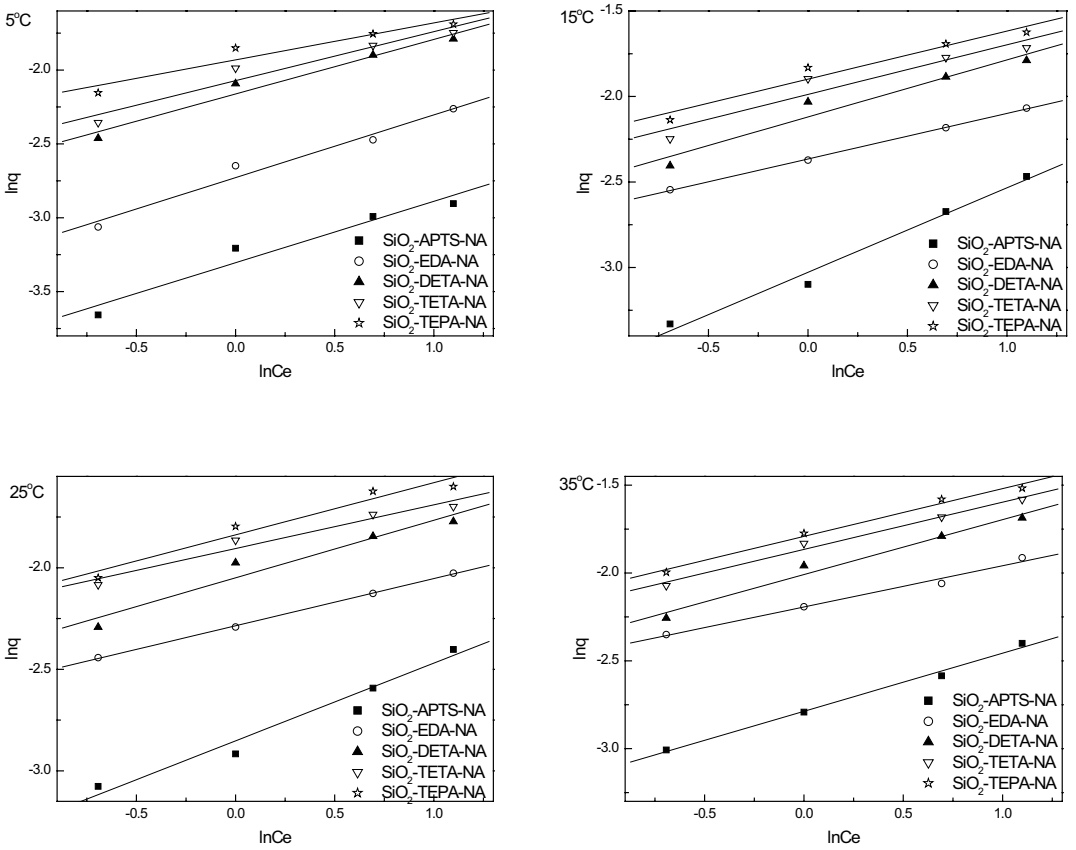


Fig. S2. Freundlich isotherms of $Cu^{2+}$ ions adsorbed on the resins at different temperature.

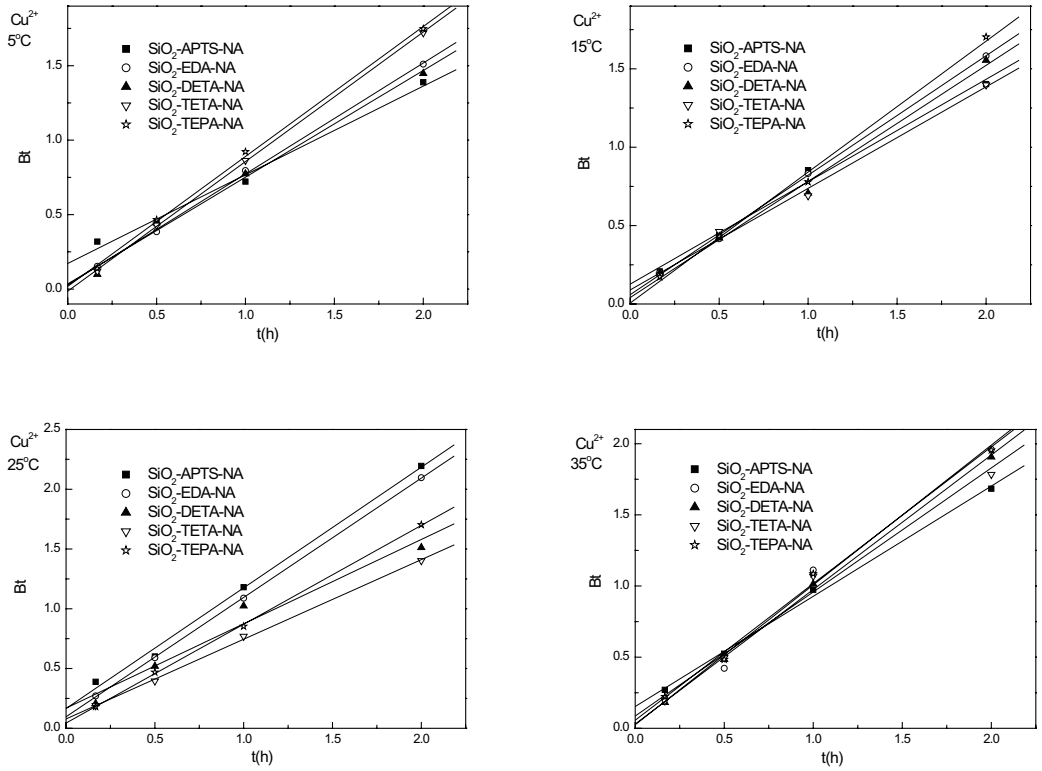


Fig. S3. $B_t$ vs. time plots at different temperatures.

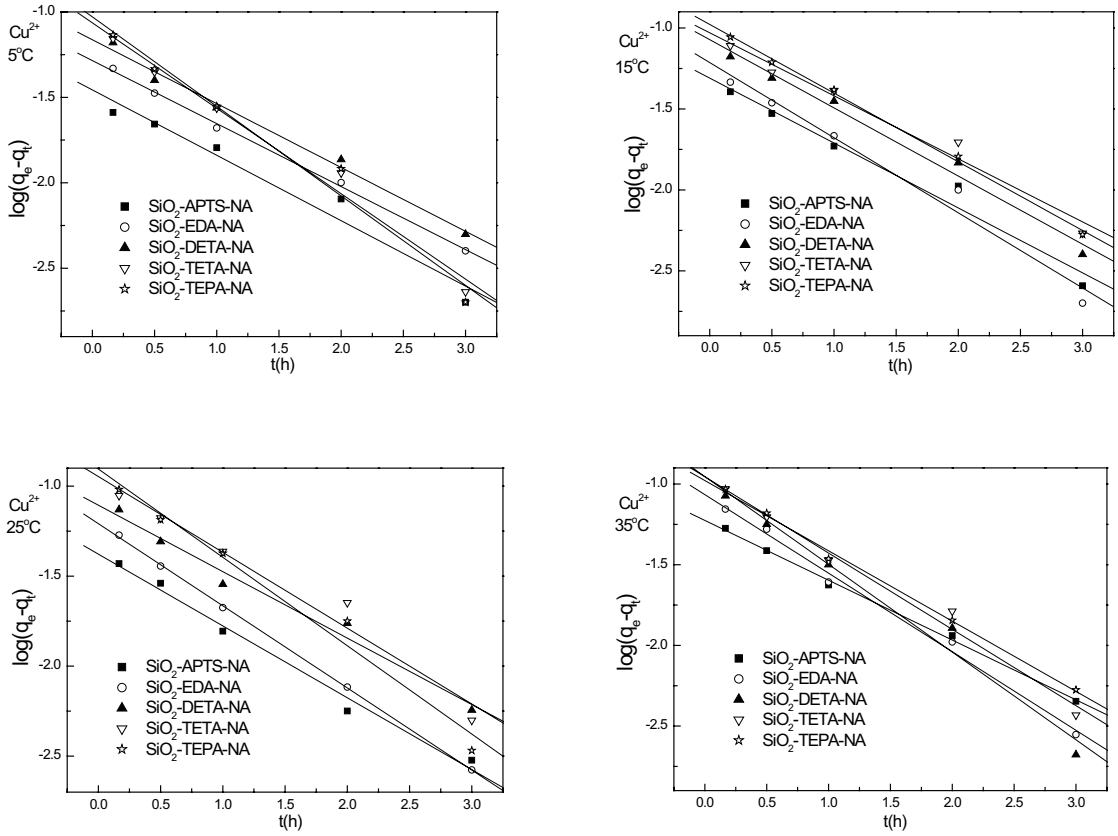


Fig. S4. Pseudo-first-order kinetic plots for the adsorption of $Cu^{2+}$ ions onto the resins at different temperatures.